Preparation and characterisation of a bis-μ-hydroxo-Ni^{III}_2 complex

Giuseppe Spedalotto,[a] Robert Gericke,[a] Marta Lovisari,[a] Erik R. Farquhar,[b] Brendan Twamley,[a] Aidan R. McDonald*[a]

Abstract: Hydroxide bridged high-valent oxidants have been implicated as the active oxidant in methane monooxygenases and other oxidases that employ bimetallic clusters in their active site. In order to understand the properties of such species, bis-μ-hydroxo-Ni^{II}_2 complex (**1**) supported by a novel dicarboxamidate ligand (N,N'-bis(2,6-dimethyl-phenyl)-2,2-dimethylmalonamide) was prepared. **1** contained a diamond core made up of two Ni^{II} ions and two bridging hydroxide ligands. Titration of the $1e^-$ oxidant $(NH_4)_2[Ce^{IV}(NO_3)_6]$ with **1** at -45 °C showed the formation of the high valent species **2** and **3**, containing $Ni^{II}Ni^{III}$ and Ni^{III}_2 diamond cores, respectively, maintaining the bis-μ-hydroxide core**.** Both complexes were characterized using electron paramagnetic resonance, X-ray absorption, and electronic absorption spectroscopies. Density functional theory computations supported our spectroscopic assignments. Oxidation reactivity studies showed that bis-μ-hydroxide-Ni^{III}_2 **3** was capable of oxidizing substrates at -45 °C at rates greater than the most reactive bis-μ-oxo-Ni^{III} complexes reported to date.

Introduction

Mono- and di-nuclear high valent metal–oxygen adducts are powerful oxidants and have been invoked to be the key oxidising intermediates in the catalytic cycles of several metalloenzymes,[1] including cytochrome P450 oxidases, Rieske dioxygenases, tyrosinase and particulate Methane Monooxygenase (pMMO, notably able to catalyse the conversion of methane to methanol).[1b, 2] Fascinatingly, recent spectroscopic analyses of the putative active oxidant in soluble methane monooxygenase (sMMO) would suggest that a bis-μ-oxo-Fe^{IV}_2 diamond core is not the active oxidant, but possibly a hydroxide bridged diiron entity facilitates CH_4 oxidation.[3] Notably, there is a dearth of synthetic hydroxide bridged high-valent oxidants in the literature.

A number of biomimetic high-valent Mn[4] and Fe[5] complexes containing both terminal and bridging oxygen ligands, have been synthesized. However, theoretical calculations predict that complexes based on later transition metals, such Co, Ni, and Cu, are expected to be more powerful oxidants.[6] Indeed one computational report predicted that Ni–O adducts would be the most potent of such oxidants.[6]

[a] G. Spedalotto, Dr. R. Gericke, M. Lovisari, Dr. B. Twamley and Dr. A. R. McDonald
School of Chemistry, Trinity College Dublin, The University of Dublin, College Green, Dublin 2 (Ireland)
E-mail: aidan.mcdonald@tcd.ie.
[b] Dr. E. R. Farquhar
Case Western Reserve University Center for Synchrotron Biosciences, National Synchrotron Light Source II, Brookhaven, National Laboratory, Upton, NY 11973 (USA)

Supporting information for this article is given via a link at the end of the document.

In an effort to explore the proposed superior reactivity of high-valent Ni oxidants, our group recently reported several examples of mononuclear terminal Ni^{III}–OX adducts (OX= O_2CCH_3, OCO_2H, ONO_2).[7] Company and co-workers isolated a putative mononuclear Ni^{III}–oxyl adduct,[8] as well as a putative mononuclear Ni^{IV}–OCl species, that were able to perform hydrogen and oxygen atom transfer reactions.[9] Ray and co-workers reported a terminal mononuclear Ni^{III}–oxygen adduct supported by a tris[2-(N-tetramethylguanidyl)ethyl]amine (TMG_3tren) ligand.[10] Several examples of high valent bis-μ-oxo-Ni^{III}_2 complexes have also been reported. Hikichi isolated and structurally characterised the first example of a bis-μ-oxo-Ni^{III}_2 complex, supported by a hydro-tris-(pyrazolyl)borate ligand.[11] Fukuzumi and Itoh[12] expanded our understanding of bis-μ-oxo-Ni^{III}_2, demonstrating their ability to carry out phenolic O–H bond and aliphatic C–H bond hydrogen atom transfer. Riordan reported the first examples of bis-μ-oxo-Ni^{III}_2 supported by thiolate ligands.[13] More recently, Browne and co-workers reported the first example of a metastable dinuclear tris-μ-oxido-Ni^{IV} complex.[14] To the best of our knowledge no hydroxide-bridged high-valent Ni_2 complexes have been reported to date, and there is limited insight into the reactivity properties of any hydroxide bridged high-valent oxidants. Herein, we report the synthesis, characterization, and reactivity properties of bis-μ-hydroxo-$Ni^{II}Ni^{III}$ and bis-μ-hydroxo-Ni^{III}_2 complexes.

Results and Discussion

Synthesis and characterization of LH_2. LH_2 (N,N'-bis(2,6-dimethyl-phenyl)-2,2-dimethylmalonamide, ^{Me_2}DMMA) was synthesized (Scheme S1, see the Supporting Information for details) by converting diethylmalonate to 2,2-dimethyl-diethylmalonate[15] and subsequent hydrolysis to the corresponding 2,2-dimethyl-malonic acid. The acid was activated

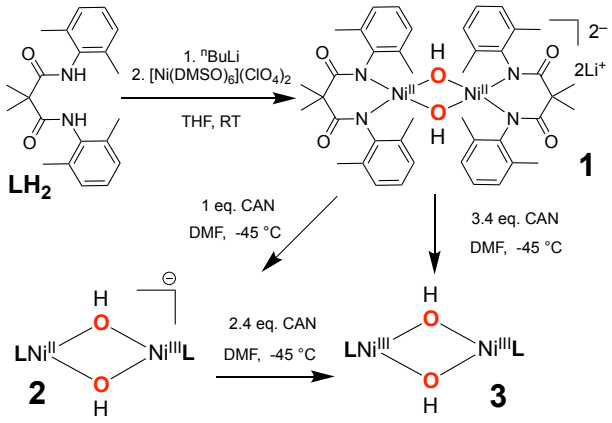

Scheme 1. Synthesis of complex of **1** and oxidation to **2** and **3** by $(NH_4)_2[Ce^{IV}(NO_3)_6]$ (CAN) at -45 °C in N,N-dimethylformamide (DMF).

as the di-acid chloride,[16] which was reacted with 2,6-dimethylaniline to yield LH_2, which was isolated in 10% overall yield. LH_2 was characterized by electrospray ionisation mass spectrometry (ESI-MS), ^1H and ^{13}C nuclear magnetic resonance, (NMR) spectroscopy, attenuated total reflectance Fourier transform infra-red (ATR/FT-IR) spectroscopy, and X-ray diffraction (XRD) measurements (Figures S1-S6, Table S1).

Synthesis and characterization of $[(Ni^{II}(OH)(L))_2]^{2-}$ (1). LH_2 was reacted with n-butyl-lithium (2.5 M in hexane, 2.5 equiv.) in tetrahydrofuran (THF), followed by the addition of $[Ni(DMSO)_6][ClO_4]_2$[17] (1 equiv., DMSO = dimethyl sulfoxide) (Scheme 1). Upon addition of the Ni^{II} salt, a colour change from pale yellow to purple followed by precipitation of a purple crystalline material was observed. The purple solid was collected by filtration and was identified as the bis-μ-hydroxide complex $Li_2[Ni^{II}(OH)(L)]_2$ (**1**), isolated in 84% yield. The preparation of **1** in high yield relied on the presence of very low concentrations of adventitious H_2O in our THF solutions. However, **1** was unstable in the presence of excess H_2O.

Metathesis of Li^+ with tetraethylammonium ions (Et_4N^+) through reaction between $Li_2[Ni^{II}(OH)(L)]_2$ and Et_4NCl allowed for the growth of crystals of $(Et_4N)_2[Ni^{II}(OH)(L)]_2$ from N,N-dimethylformamide (DMF)/diethylether (Et_2O). **1** exhibited two four-coordinate Ni ions connected by two bridging hydroxide ligands, which were refined in two symmetrical positions with a 50% chemical occupancy (Figure 1, Table S2). Geometry indexes τ_4 and τ_4'[18] indicated that each Ni centre was in a distorted square-planar geometry ($\tau_4 = 0.22$, $\tau_4' = 0.21$, $\tau = 0$ square planar, $\tau = 1$ tetrahedral, Table S3). This is presumably due to the d^8 ions preference for a square planar geometry (low spin) and to the steric hindrance and rigidity of the backbone of the ligand, L. The ketone and -CH_3 functionalities of the ligand backbone were in and out of the plane containing the core, respectively, while the 2,6-dimethylphenyl groups do not lie exactly perpendicular to the Ni(μ-OH)$_2$Ni plane (Figure S8). The average Ni–O bonds length observed in **1** (1.92 Å, Table S3) were longer than structurally analogous bis-μ-hydroxo-Ni^{II}_2 complexes based on the bidentate β-diketiminate ligands (1.86 Å)[19] but shorter than bis-μ-hydroxo-Ni^{II}_2 systems with tri-dentate (1.99 Å)[12b] and tetra-dentate (2.01 Å)[20] ligands (Table S4). The increase in the denticity of the ligands in bis-μ-hydroxo-Ni^{II}_2 complexes was thus strictly correlated with a progressive elongation of the Ni–O distances. A similar trend was observed for the Ni···Ni distances (Table S4). In this case **1** displayed the shortest Ni···Ni distances (2.88 Å) between the examples reported above.

The ^1H-NMR spectrum of complex **1** exhibited an overall shift of all peaks associated with L as a result of complexation, and the disappearance of the amide N–H resonances present in LH_2 (Figures S9–S13). The NMR data showed a relatively simple spectrum with two sets of C*H*$_3$ resonances and just two aryl C*H* resonances. This would indicate a high degree of solution fluxionality in **1**, whereas the X-ray crystal structure suggested that signals associated with these protons would be non-equivalent. Moreover, a feature at -9.3 ppm, attributable to the -O*H* resonance of the μ-hydroxide ligands, was identified. The addition of a small amount of D_2O to **1**, caused the disappearance of this resonance in the ^1H NMR spectrum, presumably as result

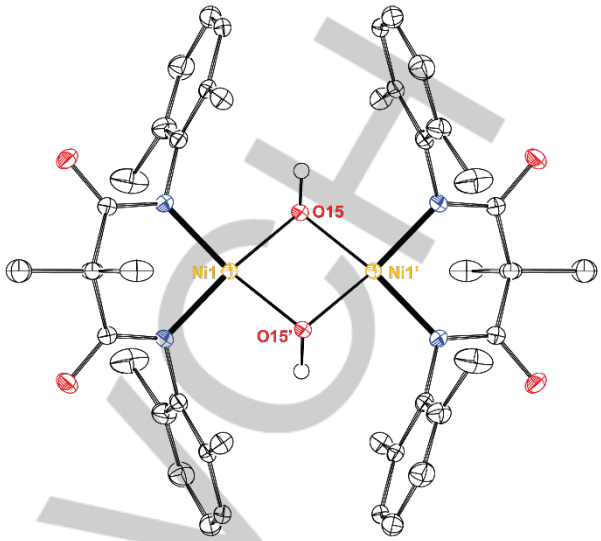

Figure 1. Symmetry generated (1-x, 1-y, 1-z) ORTEP plot of **1** showing one orientation of the bridging hydroxide, with atomic displacement at 50% probability. Counterions and co-crystallised solvent molecules were omitted for clarity as well as H- atoms, except for those associated with the μ-hydroxide ligands.

of hydrogen-deuterium exchange (Figure S10), confirming the identification of this resonance.

Further evidence of μ-hydroxide ligands was provided by ATR/FT-IR (Figure S14), which exhibited a sharp feature at ν = 3615 cm^{-1}. Such features are typical of a non-hydrogen bonded O–H stretches,[21] as previously observed by Itoh[12b] and others[22] in analogous bis-μ-hydroxo-M_2^{II} complexes (M = Mn, Co, Ni, Cu). Negative mode ESI-MS analysis showed a doubly-charged molecular ion peak at m/z = 411.1225, whose isotopic pattern and mass matched the molecular anion $[(Ni^{II}(OH)(L))_2]^{2-}$ (Figure S15), confirming the elemental composition of **1**.

Cyclic voltammetry was performed on a solution of **1** in DMF, showing the presence of two quasi-reversible waves at $E_{1/2}$ = -0.06 V ($\Delta E_{pa,pc}$ = 0.11 V) and $E_{1/2}$ = 0.24 V ($\Delta E_{pa,pc}$ = 0.12 V) vs Fc^+/Fc (Figure S16, Fc = ferrocene). The number of electrons involved in each redox event was estimated by comparing the $\Delta E_{pa,pc}$ of each wave to a standard Fc solution (see Table S5), defining this system to be a two e^- oxidation in which every oxidation event occurred stepwise. The first oxidation event was assigned to the $1e^-$ oxidation of **1** (Ni^{II}_2) to a putative mixed-valent $Ni^{II}Ni^{III}$ species (defined as **2**), followed by a subsequent $1e^-$ oxidation to a putative high valent Ni^{III}_2 species (defined as **3**). Zhou and co-workers[23] observed similar multiple $1e^-$ oxidations of a triple *meso*-helicate Ni_2 complex from $Ni^{II}_2 \rightarrow Ni^{II}Ni^{III} \rightarrow Ni^{III}_2$ and, at higher potential, from $Ni^{III}_2 \rightarrow Ni^{III}Ni^{IV} \rightarrow Ni^{IV}_2$. For bis-μ-hydroxo-$Ni^{II}_2$ complexes, Itoh and co-workers[12b] reported no stepwise oxidation in cyclic voltammetry experiments, observing only a single $1e^-$ oxidation from Ni^{II}_2 to $Ni^{II}Ni^{III}$, presumably due to the instability of the high valent bis-μ-oxo-Ni^{III}_2 state, which required low temperature (-90°C) to be observed. The voltammetric observation of a $Ni^{II}Ni^{III} \rightarrow Ni^{III}_2$ (**2** → **3**) oxidation in

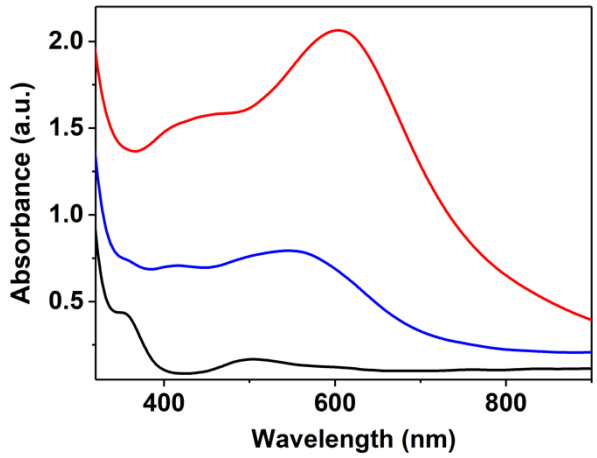

Figure 2. Electronic absorption spectroscopy monitored titration of (NH4)2[CeIV(NO3)6] (CAN) with complex **1** (black trace, DMF, -45˚C) to yield **2** (blue trace, 1.0 equiv. CAN) and **3** (red trace, 3.4 equiv. CAN).

this work highlights a remarkable accessibility of the high valent Ni^{III}_2 state, presumably as result of the stabilising contribution of the anionic donors of L.

Preparation and characterization of high-valent complexes. Titration of $(NH_4)_2[Ce^{IV}(NO_3)_6]$ (CAN) into a solution of **1** (0.2 mM, DMF, -45 °C) resulted in an immediate reaction as evidenced by electronic absorption spectroscopy (Figures 2, S18). The addition of up to one equivalent of CAN resulted in a new compound, **2** (Scheme 1), with a broad absorption feature at λ_{max} = 560 nm and a shoulder at λ_{max} = 430 nm. **2** was relatively stable at -45 °C, demonstrating a half-life of 2700 s. If complex **1** (0.2 mM, DMF, -45 °C) was reacted with one equivalent of CAN, added all at once, the instantaneous formation of **2** was observed in similar yields to that observed under sub-stoichiometric additions (Figure S19). When more than one equivalent of CAN was added to the reaction mixture (Figure 2), a second species was identified (**3**, λ_{max} = 600 nm), the maximum yield of which was obtained when 3.4 equivalents of CAN were added. **3** was less stable than **2**, demonstrating a half-life of 1500 s at -45 °C. Furthermore, when more than 3.4 equivalents of CAN were added to the reaction mixture, **3** was observed to display accelerated decay, suggesting it was unstable in the presence of excess CAN. **3** could also be prepared in the same yield by the one-time addition of 3.4 equiv. of CAN to **1** (0.2 mM, DMF, -45 °C, Figure S20).

Electronic absorption features for mono- and di-nuclear Ni^{III}–O compounds are spread over a wide range of values. Mononuclear Ni^{III}–OX complexes (OX = OCO_2H, O_2CCH_3, ONO_2) supported by 2,6-pyridinecarboxamidate ligands exhibited two main features at λ_{max} = 510-560 nm (ϵ = 6000-7000 $M^{-1}cm^{-1}$) and λ_{max} = 760-890 nm (ϵ = 3300-4600 $M^{-1}cm^{-1}$).[7] A putative Ni^{III}–oxyl system based on a bis-carboxamidate macrocyclic ligand showed instead a single band at λ_{max} = 420 nm (ϵ > 7000 $M^{-1}cm^{-1}$) and a weak shoulder at λ_{max} = 580 nm (ϵ > 800 $M^{-1}cm^{-1}$).[8] The spectra obtained for **2** and **3** are thus comparable with high-valent Ni ions supported by carboxamidate donor ligands, leading us to conclude that **2** and **3** contain $Ni^{II}Ni^{III}$ and Ni^{III}_2 cores, respectively. Previously reported bis-μ-oxo-Ni^{III}_2 complexes exhibited a common single transition in a narrow range around λ_{max} = 400–410 nm (Fukuzumi *et al.*[12b] λ_{max} = 408 nm ϵ = 6000 $M^{-1}cm^{-1}$; Itoh *et al.*[12a] λ_{max} = 405 nm ϵ = 5000 $M^{-1}cm^{-1}$; Suzuki *et al.*[24] λ_{max} = 409 nm ϵ = 3800 $M^{-1}cm^{-1}$). Riordan and co-workers reported a bis-μ-oxo-Ni^{III}_2 species showing two intense features at λ_{max} = 403 nm (ϵ = 12000 $M^{-1}cm^{-1}$) and λ_{max} = 565 nm (ϵ = 12000 $M^{-1}cm^{-1}$).[25] In the light of these reported examples, the lack of any characteristic feature at ~ 405 nm for **2** and **3** indicated the absence of the bis-μ-oxo-Ni^{III}_2 core, suggesting the presence of hydroxide ligands.

Negative-mode ESI-MS performed on a just-thawed solution of **3** detected a doubly-charged species at m/z = 410.1195, whose mass and isotopic pattern were compatible with a doubly charged doubly de-protonated species $([Ni^{III}(O)(L))_2]^{2-}$, Figure S21). The absence of any pattern related to **1** at m/z = 411.1225 suggested the full conversion of **1** in the oxidation reactions. The observation of the doubly deprotonated ion indicates that deprotonation of the complex allows for its detection by ESI-MS.

X-band electron paramagnetic resonance (EPR) spectra of frozen-solutions of **1**, **2**, **3**, *and* the titration of **1** with CAN in DMF were measured at 77 K (Figure 3). **1** exhibited a silent EPR spectrum, as expected for a Ni^{II}_2 complex in a *pseudo*-square planar geometry. Despite the expected unpaired electrons on each d^7 Ni^{III} ion, the spectrum of **3** was also EPR silent in the X-band EPR (perpendicular mode) at 77 K. This suggests the presence of magnetic coupling between the two Ni^{III} ions. A similar phenomenon was also observed by Itoh and co-workers, that reported the first example of bis-μ-oxo-Ni^{III}_2 complex with ferromagnetic coupling between high valent Ni^{III} ions (S = 1, g ~ 4 obtained by parallel mode EPR).[12a]

The EPR spectrum of **2** can be assigned to an S = ½ species (Figure 3), that we attributed to a mixed-valent $Ni^{II}Ni^{III}$ species. The signal displayed rhombic anisotropy with g_x = 2.45, g_y = 2.34, and g_z = 2.00 (Figure S22). The average g value (g_{av} =

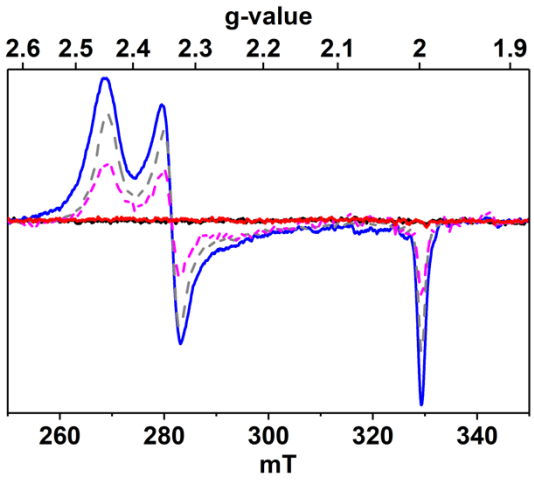

Figure 3. X-band EPR-monitored titration of CAN with **1** (black trace): 1.0 eq (**2**, blue trace), 1.5 eq (grey trace) 2.0 eq (pink trace) and 3.4 eq (**3**, red trace). Each X-band EPR spectrum was acquired from a frozen DMF solution, measured at 77 K, 6.36 mW or 2.01 mW microwave power, with 0.3 mT modulation amplitude.

2.26), alongside the rhombic anisotropy of the signal ($g_x > g_y >> g_z$), suggested the unpaired electron being localized on the metal centres, corroborating the presence of a low-spin d^7 Ni^{III} ion in a square planar or tetragonally distorted *pseudo*-octahedral coordination environment.[26] Therefore, this observation excluded the likelihood of a ligand-based radical. The yield of conversion of **1** into **2** was estimated to be 90 ± 20% by double integration of the signal and comparison with the radical standard (2,2,6,6-tetramethylpiperidin-1-yl)oxyl (TEMPO). Furthermore, the clear conversion of the EPR-active species **2** into the EPR-silent species **3** after addition of more than one equivalent of CAN (Figure 3) corroborated our observations made by electronic absorption spectroscopy and cyclic voltammetry. This high-yield formation of **2** with one equivalent of CAN followed by the disappearance of **2** with the further addition of equivalents of CAN demonstrates that **2** is a precursor to **3** and that **3** is one oxidising equivalent above **2**.

Ni K-edge X-ray absorption spectroscopic studies were performed on frozen samples of **1**, **2**, and **3**. Evaluation of the X-ray absorption near edge structure (XANES) spectra showed that the K-edge energies of the complexes were spread over a narrow range of values (Figure 4), similar to those reported for analogous Ni systems.[27] With respect to the Ni^{II}_2 precursor **1**, a shift of -0.3 eV for **2** and +0.4 eV for **3** was observed (Figure 4, Table 1). As reported by Mascharak,[27a] these edge energy shifts supply no direct evidence of oxidation state changes, reflecting instead a variation of the effective charge on the Ni centres. The edge can be influenced by core-to-valence transitions that will distort the definition of the edge energy. Indeed, we have observed similarly non-existent or small 'edge' energy shifts for mononuclear Ni complexes upon oxidation from Ni^{II} to Ni^{III}.[7, 27b]

All three species exhibited a weak pre-edge feature at 8333.2 eV (**1**), 8333.2 eV (**2**) and 8334.0 eV (**3**), assigned to an electronic-dipole forbidden 1*s*-to-3*d* transition,[27a] that in centrosymmetric point groups such as D_{4h} (square planar)[28] gains intensity from *p*/*d* mixing due to deviations from centrosymmetry.[29] Little-to-no difference was observed between the pre-edge energies of this feature for complexes **1** and **2**, while complex **3** exhibited a distinct blue shift of ~0.8 eV. The shift observed reflected a clear change in the ligand field (and possibly oxidation state) between **1**/**2** and **3**.[30]

Pre-edge areas for the compounds were calculated (Figure S24, Table 1, Table S6) revealing a ~50% increase of the area for **3** compared to **1**, presumably as a result of an increase in *d*-orbital holes in the higher-valent species **3**. Such differences in areas was reported to be a fingerprint feature of Ni^{II}/Ni^{III} couples, identifying **3** as a fully oxidised Ni^{III}_2 species.[27a] No appreciable change in the area was observed for **2**. The broad-double-bump feature approximately 5–8 eV below the edge exhibited by **1** and **2** is distinctive of four-coordinated square planar complexes[7, 27a, 31] and has been assigned to a 1*s*-to-4p_z transition.[27a] Complex **2** exhibited a less intense feature than **1**, suggesting a partial loss of square planar geometry. The absence of the feature in **3** strongly supports a drastic change in the geometry of the two Ni^{III} centres, suggesting the presence of *pseudo*-octahedral environment.

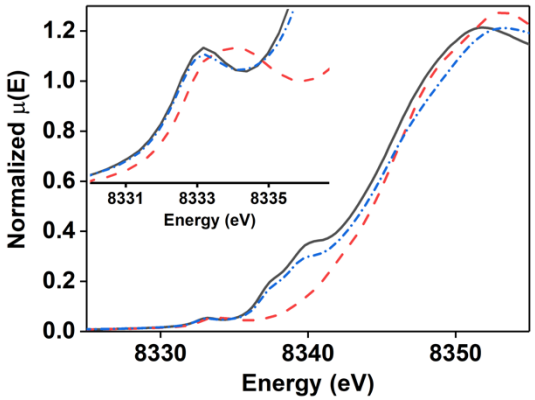

Figure 2. Normalized Ni K-Edge XANES spectra of **1** (solid black line), **2** (dash-dotted blue line), **3** (dashed red line). Inset: Pre-edge region.

Extended X-ray absorption fine structure (EXAFS) analysis of **1** demonstrated negligible differences from the crystallographic data (Tables 1, S7, Figure S26). The best fit showed the presence of a first coordination shell composed of 4 N/O scatterers, divided in subshells of 2 scatterers at 1.88 Å and 2.03 Å each, matching well with X-ray diffraction measurements (Table S8). Several attempts were made to fit the second coordination shell with light atoms, revealing the necessity of a heavier atom to improve the fit. A second Ni atom was refined at 3.09 Å, a value 0.2 Å longer than XRD data reported above (Table S8). The

presence of a heavy atom scatterer was also evaluated by the k^5-weighted Fourier transform in EXAFS analysis. The intensity of FT peaks from a heavier scatterer is dependent on *n* (in k^n) and is expected to increase going from k^3 (normally used for EXAFS analysis) to k^5.[32] The k^5-weighted Fourier transform for **1** (Figure S25) showed a clear increase in the FT magnitude in the region 2.6-3.0 Å, defining the presence of a heavier scatterer (i.e. the second Ni atom). The shell was completed by 4 C atoms at 2.87 Å from the ligand backbone.

The best fit for the EXAFS analysis of **2** (Tables 1, S9, Figure S26) showed a first coordination shell composed of 4 N/O atoms, at 1.89 Å (Table S9). The second coordination shell refined the second Ni atom at 2.86 Å, representing a shorter Ni···Ni distance with respect to **1**. Such a decrease could be ascribed to a formal oxidation state change of +1 when compared to **1**.

EXAFS analysis of **3** initially showed a best fit of six N/O scatterers in the first coordination shell, divided in two sub-shells composed of 3 N/O atoms each at 1.93 Å and 2.05 Å (Table 1, S10, Figure S26). DFT calculations performed excluded this possibility because steric crowding around the Ni_2 core prevented two solvent molecules binding to each Ni^{III} atom (*vide infra*). Therefore, EXAFS fitting with penta-coordination was explored, showing a first coordination sphere composed by five N/O scatterers, divided in two sub-shells made by 4 N/O atoms at 1.95 Å and 1 N/O(DMF) atom lying at 2.08 Å. These values were in agreement with the distances gathered by DFT

Table 1. Significant data from Ni K-edge X-ray absorption spectroscopy analysis of complexes **1**, **2**, and **3** and comparison with the predicted distances[a] obtained by DFT calculations[d].

	E_{edge}[b]	$E_{pre\text{-}edge}$[b]	$Area_{pre\text{-}edge}$[c]	Ni–N/O	Ni···O_{DMF}	Ni···Ni
1	8345.7	8333.2	5.65(5)	2 N @ 1.88 2 O @ 2.03		3.09
2	8345.4	8333.2	5.54(29)	4 @ 1.89	-	2.85
2				*4 @ 1.88*	-	*2.86*
2-oxo				*4 @ 1.88*	-	*2.69*
3	8346.1	8334	11.55(36)	4 @ 1.95	2.08	2.97
3				*4 @ 1.92*	*2.07*	*3.00*
3-oxo				*4 @ 1.85*	-	*2.70*

[a] Distances reported in Å. [b] Energy values reported in eV. [c] Areas multiplied by 100 for convenience. [d] DFT predicted models are highlighted in Italic.

calculations (Table 1, S12). The calculated metal-ligand bond distances for **3** were longer compared to **1** and **2**, defining a significant expansion of the first shell presumably caused by expanding the coordination number from four to five. A heavy atom scatterer (*i.e.* the second Ni atom, 2.97 Å) was required to improve the fit, as also confirmed by k^5-weighted Fourier transform (Figure S25).[32] The EXAFS analysis of **3** nicely corroborates XANES observations, confirming a change in the coordination geometry.

The Ni–O bond length and the Ni···Ni distance are topical parameters to identify the nature of the bridging ligands, allowing us to gauge whether **2** and **3** maintains the bis-μ-hydroxide core or has converted to a bis-μ-oxo core. The presence of a bridging oxo-ligands would be expected to result in shorter Ni–O and Ni···Ni distances. Comparison of the distances in **3** with the few structurally characterised bis-μ-oxo-Ni^{III}_2 complexes exhibited stark differences. Even considering the elongation due to the change in coordination number in **3**, the Ni–O bond length of 1.95 Å obtained for **3** was longer than the reported average values for bis-μ-oxo cores of ~1.87 Å, suggesting the presence of hydroxide ligands.[11-12, 33] Additionally, the refined Ni···Ni distance (**3**, 2.97 Å; bis-μ-oxo-Ni^{III}_2, 2.86–2.92 Å[11-12, 33]) would also suggest a bis-μ-hydroxide core.

Quantum chemical calculations at the DFT uBP86-D3-cc-pVTZ (C, H, N, O) / SDD (Ni) level of theory were performed to give theoretical support for the XAS-measured structures and geometries of complexes **1**, **2**, and **3** and their homologous μ-oxo-bridged complexes **1-oxo**, **2-oxo**, and **3-oxo**. The geometry optimized structures of the μ-oxo complexes **1-oxo**, **2-oxo** and **3-oxo** (Table 1) showed that the average Ni–O bond lengths were 1.79 Å which is shorter (0.08-0.24 Å) than what was measured and computationally predicted for hydroxide complexes **1**, **2**, and **3** (Tables 1, S12). Furthermore, the Ni···Ni distances were predicted to be 2.68 (**1-oxo**), 2.69 (**2-oxo**), and 2.70 (**3-oxo**) Å, which are again significantly shorter by about 0.27-0.40 Å compared to those predicted and measured for hydroxide complexes **1**, **2**, and **3** (Table 1, S12). This provides convincing proof that the hydroxide ligand has been maintained in complexes **2** and **3**.

We then used DFT calculations to understand the Ni-ligand coordination number and geometry in complexes **2** and **3**. The single crystal X-ray molecular structure of **1** reveals two possible hydroxide orientations causing a seesaw or planar Ni(μ-$OH)_2$Ni core (Figure S8). The geometry optimised structures of **1**, **2**, and **3** exhibit the seesaw configuration to be more stable by 2.01 kcal·mol^{-1} for **1**, 1.44 kcal·mol^{-1} for **2**, while for **3** the seesaw configuration was the only structure obtained. The differences in Ni–O and Ni–N bond lengths in the planar or seesaw configurations were small (Table S12) indicating that the exact configuration was not consequential for an understanding of the EXAFS results.

Geometry optimizations with or without one DMF coordinated to **2** have been performed (Table S12). A better match with the EXAFS results was obtained for the structure without a DMF ligand bound to the complex, which is also consistent with the XANES results that indicated a square planar coordination environment around the Ni ions. DFT thus supports the postulate that the Ni ions remain four-coordinate upon one electron oxidation of **1** to yield **2**.

The average Ni–N/O and Ni···Ni distances (Table S12) of geometry optimized structures for **3**, without a DMF ligand bound to the Ni ions, were slightly shorter when compared to the results found by EXAFS (Table 1). The geometry optimized structure of **3** *with* coordinated DMF molecules (see supporting information for details on Ni/DMF interaction, Table S12) was instead in very good agreement with the EXAFS findings. Overall, DFT supports the structures of **2** and **3** contain bis-μ-hydroxide cores, and affirms the EXAFS predicted Ni-ligand and Ni···Ni distances (Table 1).

For **2**, the Mulliken spin density plot showed spin density located at both Ni cores (0.33, 0.34) with predominant d_{xz} character (Figure S39). For **3** calculations showed that both the S = 1 and S = 0 states were stable, with neglible difference in energy (0.12 kcal·mol^{-1}). The Mulliken spin density plots for **3** showed two Ni^{III}

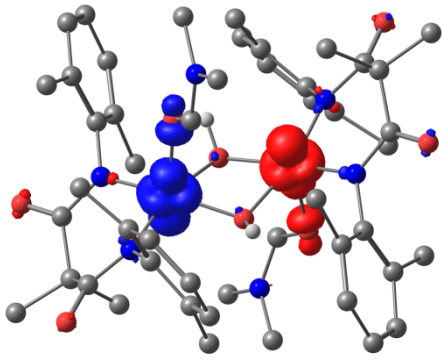

Figure 5. Geometry optimised structures of **3** (anti-ferromagnetic coupled singlet) at an iso-value of 0.01 a.u., with electron spin density plotted. H- atoms omitted for clarity, except those associated with the μ-hydroxide ligands.

centers (triplet: 0.909, 0.918; singlet: 0.900, -0.912) with mainly d_{z2} character (Figures 5, S39).

Reactivity studies. The oxidation reactivity of both **2** and **3** towards substrates containing weak X–H (X = C, O) bonds was explored. An important observation was that **2** was formed from the reaction between **3** and external substrate. **2** decayed further at a significantly lower rate, *after* **3** had decayed (Figure S27). We measured the kinetics of substrate oxidation of **2** and **3** independently, by preparing them separately. For **3** only the first phase of decay upon addition of substrate was analysed.

At -45 °C 4-methyl-2,6-di-*tert*-butyl-phenol (4-CH_3-2,6-DTBP) reacted readily with both complexes. The kinetics of the reactions were studied by electronic absorption spectroscopy, monitoring the feature at λ_{max} = 560 nm for **2** and λ_{max} = 600 nm for **3**. The decay was fitted as *pseudo*-first order (yielding k_{obs}) and a plot of k_{obs} against [substrate] gave the second order rate constant (k_2). For the reaction between **2** and 4-CH_3-2,6-DTBP at -45 °C, k_2 = 0.76(4) $M^{-1}s^{-1}$ (Figure S29) was measured. For the reaction between **3** and 4-CH_3-2,6-DTBP, under the same conditions, k_2 = 24.7(11) $M^{-1}s^{-1}$ was calculated (Figures S30). ESI-MS analysis of the post-reaction mixtures revealed the presence of 2,6-di-*tert*-butyl-4-methylenecyclohexa-2,5-dien-1-one for both high-valent oxidants (Figures S31-S32). This product formed as result of hydrogen atom abstraction from the substrate, indicating some form of proton coupled electron transfer (PCET) oxidation of the phenol O–H bond had occurred. Comparing the k_2 for both high-valent oxidants showed that **3** was 30-fold more reactive than **2**, suggesting that the higher oxidation state of **3** imbues it with higher rates of reaction.

The kinetic isotopic effect (KIE) was measured for both complexes by reaction with 4-CH_3-*[D]*-2,6-DTBP and comparison with the data previously obtained with 4-CH_3-*[H]*-2,6-DTBP. **2** exhibited a KIE of ~ 2 (Figure S35-S36), while **3** showed a value of ~ 4 (Figure S37-38) defining the cleavage of the phenolic O–H bond as the likely rate determining step. Critically, the KIE values obtained for **2** and **3** were considerably smaller than those reported for analogues oxo-ligated complexes: bis-μ-oxo-Ni^{III}_2 (KIE = 21.4),[12b] bis-μ-oxo-Cu^{III}_2 (KIE = 26-40)[34] and bis-μ-oxo-$Fe^{III}Fe^{IV}$ (KIE = 20)[35]. In these complexes, and often for terminal metal-oxo's (M=O), tunnelling has been attributed to the hydrogen atom transfer mechanism resulting in exceptionally high KIE values. In contrast for M–O–X oxidants KIE values are almost always less than the classical limit of 7, ruling out a tunnelling mechanism.[36] This observation points towards complexes **2** and **3** having hydroxide and not oxo- ligands.

2 and **3** were also reacted with 2,4-di-*tert*-butyl-phenol (2,4-DTBP). k_2 values of 0.18(1) $M^{-1}s^{-1}$ and 23.8(6) $M^{-1}s^{-1}$, respectively, were calculated (Figures S33-S34). Comparison of the obtained k_2 values with previously reported bis-μ-oxo-Ni^{III}_2 complexes shows that **3** was more reactive than any bis-μ-oxo-Ni^{III}_2 complex reported to date (Table 2).

3 also reacted with 9,10-dihydroanthracene (DHA, Figure 6). **2** was not capable of oxidising DHA, however **2** was also formed as a result of oxidation of DHA by **3**. The k_{obs} for DHA oxidation by **3** were close to the self-decay rate of **3**, making calculation of a k_2-value under the current experimental conditions inaccurate.

Table 2. Comparison of reactivity of **2** and **3** with 2,4 di-*tert*-butylphenol against bis-μ-oxo-Ni^{III}_2 complexes.

Compound	T (°C)	k_2 ($M^{-1}s^{-1}$)
2	-45	0.18(1)
3	-45	23.8(6)
$[(L_1^H)Ni^{III}(\mu\text{-}O)_2Ni^{III}(L_1^H)]^{2+}$	-50	1.08 [12b]
$[(dpema)Ni^{III}(\mu\text{-}O)_2Ni^{III}(dpema)]^{2+}$	-60	13 [12a]

L1H = N,N'-bis[2-(2-pyridyl)ethyl]-2-phenylethylamine; dpema = N,N-(di-[2-pyridine-2-yl]ethyl)methylamine.

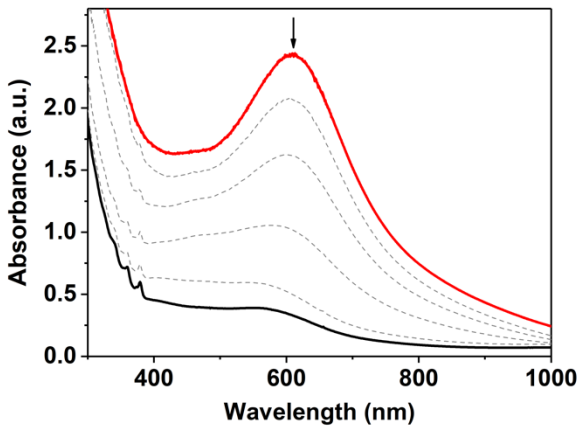

Figure 6. Electronic absorption spectra changes upon reaction of **3** with 9,10-dihydroanthracene (200 equiv.) at -45 °C in DMF.

Features for the anthracene product were identified using electronic absorption spectroscopy (λ = 360, 379 nm, Figure 6), confirming oxidation of DHA had occurred.[37] Furthermore, gas chromatography (GC) analysis allowed us to identify anthracene in the post-reaction mixture obtained in ~80% yield (Figure S32, Table S11), demonstrating that 3 was capable of activating weak C–H bonds at -45 °C.

Conclusions

The bis-μ-hydroxo-Ni^{II}_2 complex (**1**) supported by a novel malondiamidate ligand was prepared and characterised. **1** contained a diamond core structure composed of two Ni atoms and two bridging hydroxide ligands. **1** was converted to a mixed valent bis-μ-hydroxo-$Ni^{II}Ni^{III}$ complex (**2**) *and* a high valent bis-μ-hydroxo-Ni^{III}_2 complex (**3**). These species represent the first examples of high valent bis-μ-hydroxo-Ni_2 complexes. Both **2** and **3** were capable of performing oxidation of phenolic O–H bonds. Critically, **3** displayed k_2-values higher than any reported bis-μ-oxo-Ni^{III}_2 complex reported to date and was also capable of activating weak C–H bonds. These results demonstrate that high-

valent hydroxide-bridged dinuclear clusters are capable oxidants and match the kinetic reactivity of the most reactive comparable oxo-bridged entities, turning the tables in the current understanding of the activity of several metallo-enzymes. We continue to explore the reactivity properties and mechanism of oxidation by these complexes and their relevance to biological diamond core clusters.

Acknowledgements

This publication has emanated from research supported by European Research Council (ERC-2015-STG-678202). Research in the McDonald lab is supported in part by a research grant from Science Foundation Ireland (SFI/15/RS-URF/3307). XAS experiments were conducted at SSRL beamline 7-3 (SLAC National Accelerator Laboratory, USA), with support from the DOE Office of Science (DE-AC02-76SF00515), DOE Office of Science Office of Biological and Environmental Research and NIH (P41-GM-103393 and P30-EB-009998). We are grateful to COST Action CM1305 (ECOSTBio) for networking support. We thank Prof. Robert Barkley for training on and use of an EPR spectrometer. We wish to acknowledge the Irish Centre for High-End Computing (ICHEC) for the provision of computational facilities and support.

Keywords: high-valent oxidant • diamond core • bis-μ-hydroxo-Ni_2 • hydrocarbon oxidation • bioinorganic chemistry

[1] a) L. Que, Jr., W. B. Tolman, *Nature* **2008**, *455*, 333-340; b) M. O. Ross, A. C. Rosenzweig, *J. Biol. Inorg. Chem.* **2017**, *22*, 307-319.

[2] S. Sirajuddin, A. C. Rosenzweig, *Biochemistry* **2015**, *54*, 2283-2294.

[3] G. E. Cutsail, 3rd, R. Banerjee, A. Zhou, L. Que, Jr., J. D. Lipscomb, S. DeBeer, *J Am Chem Soc* **2018**, *140*, 16807-16820.

[4] a) C. Deville, S. K. Padamati, J. Sundberg, V. McKee, W. R. Browne, C. J. McKenzie, *Angew. Chem. Int. Ed.* **2016**, *55*, 545-549; b) R. A. Baglia, K. A. Prokop-Prigge, H. M. Neu, M. A. Siegler, D. P. Goldberg, *J. Am. Chem. Soc.* **2015**, *137*, 10874-10877; c) D. E. Lansky, D. P. Goldberg, *Inorg. Chem.* **2006**, *45*, 5119-5125.

[5] a) M. Costas, M. P. Mehn, M. P. Jensen, L. Que, *Chem. Rev.* **2004**, *104*, 939-986; b) J.-U. Rohde, J.-H. In, M. H. Lim, W. W. Brennessel, M. R. Bukowski, A. Stubna, E. Münck, W. Nam, L. Que, *Science* **2003**, *299*, 1037-1039; c) J. E. M. N. Klein, L. Que, in *Encyclopedia of Inorganic and Bioinorganic Chemistry*, **2016**, pp. 1-22; d) M. R. Mills, A. C. Weitz, M. P. Hendrich, A. D. Ryabov, T. J. Collins, *J Am Chem Soc* **2016**, *138*, 13866-13869; e) W. Nam, *Acc. Chem. Res.* **2015**, *48*, 2415-2423; f) S. Hong, K. D. Sutherlin, J. Park, E. Kwon, M. A. Siegler, E. I. Solomon, W. Nam, *Nat. Commun.* **2014**, *5*, 5440; g) D. C. Lacy, R. Gupta, K. L. Stone, J. Greaves, J. W. Ziller, M. P. Hendrich, A. Borovik, *J. Am. Chem. Soc.* **2010**, *132*, 12188-12190.

[6] A. W. Pierpont, T. R. Cundari, *Inorg. Chem.* **2010**, *49*, 2038-2046.

[7] P. Pirovano, E. R. Farquhar, M. Swart, A. R. McDonald, *J. Am. Chem. Soc.* **2016**, *138*, 14362-14370.

[8] T. Corona, F. F. Pfaff, F. Acuna-Pares, A. Draksharapu, C. J. Whiteoak, V. Martin-Diaconescu, J. Lloret-Fillol, W. R. Browne, K. Ray, A. Company, *Chem. Eur. J.* **2015**, *21*, 15029-15038.

[9] T. Corona, A. Draksharapu, S. K. Padamati, I. Gamba, V. Martin-Diaconescu, F. Acuna-Pares, W. R. Browne, A. Company, *J Am Chem Soc* **2016**, *138*, 12987-12996.

[10] F. F. Pfaff, F. Heims, S. Kundu, S. Mebs, K. Ray, *Chem. Commun.* **2012**, *48*, 3730-3732.

[11] S. Hikichi, M. Yoshizawa, Y. Sasakura, M. Akita, Y. Moro-oka, *J. Am. Chem. Soc.* **1998**, *120*, 10567-10568.

[12] a) Y. Morimoto, Y. Takagi, T. Saito, T. Ohta, T. Ogura, N. Tohnai, M. Nakano, S. Itoh, *Angew. Chem. Int. Ed.* **2018**, *57*, 7640-7643; b) S. Itoh, H. Bandoh, M. Nakagawa, S. Nagatomo, T. Kitagawa, K. D. Karlin, S. Fukuzumi, *J. Am. Chem. Soc.* **2001**, *123*, 11168-11178; c) S. Itoh, H. Bandoh, S. Nagatomo, T. Kitagawa, S. Fukuzumi, *J. Am. Chem. Soc.* **1999**, *121*, 8945-8946.

[13] B. S. Mandimutsira, J. L. Yamarik, T. C. Brunold, W. Gu, S. P. Cramer, C. G. Riordan, *J. Am. Chem. Soc.* **2001**, *123*, 9194-9195.

[14] S. K. Padamati, D. Angelone, A. Draksharapu, G. Primi, D. J. Martin, M. Tromp, M. Swart, W. R. Browne, *J. Am. Chem. Soc.* **2017**, *139*, 8718-8724.

[15] H. Zhang, Y. Dong, *Pat. WO2012CN01001 20120726*, KBP BioSciences Co., Ltd., Peop. Rep. China . **2012**, p. 73 pp.

[16] W. K. Anderson, R. Kasliwal, D. M. Houston, Y.-s. Wang, V. L. Narayanan, R. D. Haugwitz, J. Plowman, *J. Med. Chem.* **1995**, *38*, 3789-3797.

[17] F. Cotton, R. Francis, *J. Am. Chem. Soc.* **1960**, *82*, 2986-2991.

[18] L. Yang, D. R. Powell, R. P. Houser, *Dalton Trans.* **2007**, 955-964.

[19] Y. Li, L. Jiang, L. Wang, H. Gao, F. Zhu, Q. Wu, *Appl. Organomet. Chem.* **2006**, *20*, 181-186.

[20] C. Jaeheung, F. Hideki, F. Shuhei, S. Masatatsu, *Angew. Chem. Int. Ed.* **2004**, *43*, 3300-3303.

[21] R. M. Silverstein, F. X. Webster, D. J. Kiemle, D. L. Bryce, *Spectrometric identification of organic compounds*, 8th ed., John wiley & sons, **2014**.

[22] a) E. Carmona, J. M. Marin, P. Palma, M. Paneque, M. L. Poveda, *Inorg. Chem.* **1989**, *28*, 1895-1900; b) N. Kitajima, S. Hikichi, M. Tanaka, Y. Morooka, *J. Am. Chem. Soc.* **1993**, *115*, 5496-5508.

[23] J. Ferrando-Soria, O. Fabelo, M. Castellano, J. Cano, S. Fordham, H. C. Zhou, *Chem. Commun.* **2015**, *51*, 13381-13384.

[24] K. Honda, J. Cho, T. Matsumoto, J. Roh, H. Furutachi, T. Tosha, M. Kubo, S. Fujinami, T. Ogura, T. Kitagawa, M. Suzuki, *Angew. Chem. Int. Ed.* **2009**, *48*, 3304-3307.

[25] R. Schenker, B. S. Mandimutsira, C. G. Riordan, T. C. Brunold, *J. Am. Chem. Soc.* **2002**, *124*, 13842-13855.

[26] a) R. I. Haines, A. McAuley, *Coord. Chem. Rev.* **1981**, *39*, 77-119; b) S. A. Jacobs, D. W. Margerum, *Inorg. Chem.* **1984**, *23*, 1195-1201.

[27] a) G. J. Colpas, M. J. Maroney, C. Bagyinka, M. Kumar, W. S. Willis, S. L. Suib, P. K. Mascharak, N. Baidya, *Inorg. Chem.* **1991**, *30*, 920-928; b) P. Mondal, P. Pirovano, A. Das, E. R. Farquhar, A. R. McDonald, *J. Am. Chem. Soc.* **2018**, *140*, 1834-1841; c) S. Kundu, F. F. Pfaff, E. Miceli, I. Zaharieva, C. Herwig, S. Yao, E. R. Farquhar, U. Kuhlmann, E. Bill, P. Hildebrandt, H. Dau, M. Driess, C. Limberg, K. Ray, *Angew. Chem. Int. Ed.* **2013**, *52*, 5622-5626.

[28] A. Roe, D. Schneider, R. Mayer, J. Pyrz, J. Widom, L. Que Jr, *J. Am. Chem. Soc.* **1984**, *106*, 1676-1681.

[29] G. Shulman, Y. Yafet, P. Eisenberger, W. Blumberg, *Proc. Natl. Acad. Sci.* **1976**, *73*, 1384-1388.

[30] J. Cho, R. Sarangi, J. Annaraj, S. Y. Kim, M. Kubo, T. Ogura, E. I. Solomon, W. Nam, *Nat. Chem.* **2009**, *1*, 568.

[31] L. R. Furenlid, M. W. Renner, E. Fujita, *Physica B Condens. Matter* **1995**, *208*, 739-742.

[32] R. A. Scott, M. K. Eidsness, *Comments Inorg. Chem.* **1988**, *7*, 235-267.

[33] K. Shiren, S. Ogo, S. Fujinami, H. Hayashi, M. Suzuki, A. Uehara, Y. Watanabe, Y. Moro-oka, *J. Am. Chem. Soc.* **2000**, *122*, 254-262.

[34] S. Mahapatra, J. A. Halfen, E. C. Wilkinson, G. Pan, X. Wang, V. G. Young, C. J. Cramer, L. Que, W. B. Tolman, *J. Am. Chem. Soc.* **1996**, *118*, 11555-11574.

[35] L. Que Jr, W. B. Tolman, *Angew. Chem. Int. Ed.* **2002**, *41*, 1114-1137.

[36] P. Pirovano, A. R. McDonald, *Eur. J. Inorg. Chem.* **2018**, *2018*, 547-560.

[37] A. Ohta, K. Hattori, Y. Kusumoto, T. Kawase, T. Kobayashi, H. Naito, C. Kitamura, *Chem. Lett.* **2012**, *41*, 674-676.

FULL PAPER

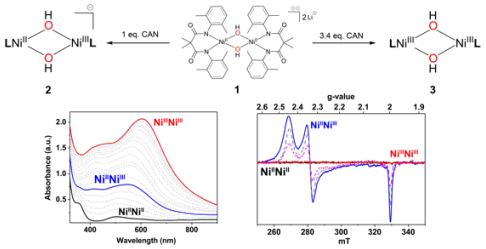

High valent bis-μ-hydroxo-Ni_2 complexes have been prepared and found to be capable of performing hydrocarbon and phenol oxidation. Critically, bis-μ-hydroxo-Ni^{III}_2 displayed k_2-values higher than any reported bis-μ-oxo-Ni^{III}_2 complex reported to date. This demonstrates that high-valent hydroxide-bridged dinuclear clusters are capable oxidants, and could be involved in metallo-oxygenases.

*Giuseppe Spedalotto, Robert Gericke, Marta Lovisari, Erik R. Farquhar, Brendan Twamley, Aidan R. McDonald**

Page No. – Page No.

Preparation and characterisation of a bis-μ-hydroxo-Ni^{III}_2 complex